JOURNAL OF NANO- AND ELECTRONIC PHYSICS
Vol. **18** No 3, 03012(6pp) (2026)

ЖУРНАЛ НАНО- ТА ЕЛЕКТРОННОЇ ФІЗИКИ
Том **18** № 3, 03012(6cc) (2026)

OPEN ACCESS

REGULAR ARTICLE

Modern CAD Tools for Single-Electron Nanodevices

O.S. Melnyk* ✉, O.O. Nahaichenko†

National University "Kyiv Aviation Institute", 03058 Kyiv, Ukraine

(Received 02 April 2026; revised manuscript received 19 June 2026; published online 26 June 2026)

This paper presents an analysis of the results obtained in the computer-aided design of nanodevices based on quantum-dot cellular automata using modern single-electronics CAD tools such as QCADesigner, QCADesigner-E, and QCADesigner-FS. Using a nanomultiplexer circuit as a case study, functional, temperature-dependent, thermo-energy, and probabilistic defect-oriented simulations were performed. It is shown that modern CAD suites make it possible not only to synthesize the topology of a nanocircuit, but also to comprehensively evaluate its operability, energy efficiency, and resistance to structural defects. It was ultimately iestablished that the investigated nanomultiplexer correctly implements the signal-selection function; however, it remains operable only within a limited cryogenic temperature range. The energy analysis revealed a periodic behavior of the dissipation components associated with the clocking phases, whereas QCADesigner-FS simulation confirmed a significant dependence of the error probability on four types of process-induced defects, the fault level, and the topological placement of cells. The most vulnerable elements were found to be the functionally critical nodes associated with signal injection, control, and output formation.

Keywords: Single-electron nanoelectronics, Computer-aided design, Cryogenic temperature, Energy dissipation, Defect tolerance of nanocircuits.

DOI: 10.21272/jnep.18(3).03012 PACS numbers: 85.35.Be, 85.35.Gv

1. INTRODUCTION

Modern micro- and nanoelectronics have entered a domain in which geometric scaling no longer guarantees either an increase in performance or a reduction in power consumption; instead, the roles of quantum effects, thermal fluctuations, process-parameter deviations, and defects increase sharply. Under such conditions, non-automated design of nanoelectronic devices becomes practically unsuitable, because the number of interdependent parameters – such as geometric dimensions, energy barriers, control modes, temperature, and noise – that must be coordinated in order to achieve functional correctness, operability, and an acceptable level of energy consumption is constantly growing.

For single-electron devices, the key point is that logic states and switching are determined by the energy of charge quantization and Coulomb interaction. For example, a single-electron transistor (SET) operates in Coulomb-blockade and tunneling regimes, which in turn require the thermal energy to be much smaller than the charging energy, $k_BT << E_c$, and the tunnel resistances to be sufficiently high with respect to the quantum resistance, $R_t \gg \frac{h}{e^2} = \frac{6.626 \cdot 10^{-34}\ \frac{J}{sec}}{2.567 \cdot 10^{-38}\ C} \approx 25.8\ kOhm$. Otherwise, thermal fluctuations and quantum processes destroy the single-electron effect and destabilize logical operation [1-3].

At the same time, in computational structures based on quantum-dot cellular automata (QCA), information is encoded not by voltage and current levels, but by the polarization of interacting cells. The operation of nanocircuits is determined by four-phase clocking used to control tunneling barriers, as well as by the level of intercell interaction [4-6]. Therefore, computer-aided design of single-electron nanodevices requires control over the circuit topology, geometry, and clock synchronization of operation, as well as over their electrophysical and energy parameters [7].

Thus, the modern challenges of automated nanodevice design consist in the need to develop a CAD ecosystem that formalizes the description of logical operation, automatically synthesizes the nanostructure and constructs its physical model, performs hierarchical verification of the design, and provides the designer with optimization criteria.

2. ANALYSIS OF PUBLICATIONS AND PREVIOUS RESEARCH

The first fundamental works on single-electron processes established the physics of Coulomb blockade, tunneling, and electric-charge quantization [1-3]. Within the computational model of quantum-dot cellular automata, the possibility of implementing logic elements through Coulomb interaction was demonstrated in [5, 6]. An important step in the transition from theory to engineering design was the emergence of rapid synthesis and simulation tools, among which QCADesigner became the principal CAD environment [8]. For the development of CAD tools for single-electron nanocircuits, a number of approaches to syn-

* Correspondence e-mail: oleksandr.melnyk@npp.kai.edu.ua
† 6937694@stud.kai.edu.ua

Cite this article as: O.S. Melnyk et al., *J. Nano- Electron. Phys.* 18 No 3, 03012 (2026) https://doi.org/10.21272/jnep.18(3).03012

thesis, simulation, and analysis have been proposed and improved, including the energy-modeling and energy-estimation approach [7, 9]; nanocircuit design and optimization approaches [10]; methods for reliability analysis and defect sensitivity [11]; algorithms for cell placement and ordering that take standard clocking zones into account [12]; new clocking-zone architectures (universal, efficient, and two-dimensional) [13-15]; tools for alternative logical approaches, in particular those based on ternary cellular automata such as TQCAsim [16]; as well as generalizing monographs and survey papers [4, 17].

Modern CAD tools help solve most of the complex tasks involved in the automated design of single-electron nanodevices; however, a number of issues remain only partially resolved. Among them is the gap between abstraction levels, because in QCA/SET systems the logical level is directly determined by such physical parameters as geometric dimensions, potential barriers, temperature, and synchronization mechanisms. This requires special models that link implementation with noise-robust operation [7, 9-11]. Another challenge is temperature- and noise-induced degradation, because a specific requirement for QCA operability is the preservation of polarization levels and correct adiabatic clock dynamics; therefore, CAD tools must automatically evaluate the operating temperature ranges of a given nanocircuit [1-3, 9]. For single-electron nanodevices, it is also fundamentally important to evaluate the components of dissipated energy, the propagation of clock pulses, the transfer and control of energy balance, and numerical integration error [7, 9]. As nanocircuit size increases, problems associated with limited signal fan-out, segment crossings, defects, and process variations arise, which requires full-system fault analysis and failure verification tools, including those implemented in QCADesigner-FS [11].

3. COMPUTER-AIDED DESIGN OF NANOCIRCUITS USING MODERN CAD SUITES

QCADesigner – is a CAD environment that makes it possible to rapidly build QCA nanocircuits and simulate their operation using different models [8]. These include, first, a fast but simplified model for the analysis of most circuits (the Bistable Approximation), and second, a more sophisticated quantum-mechanical model (the Coherence Vector Model, CVM), which more accurately reproduces the dynamic interaction between cells.

At the same time, even at the level of an individual node, the designer must coordinate geometry, clocking zones, and the simulation model; when moving to larger circuits, there arises a need for automated rules for forming clocking zones, placing elements, checking the design, and detecting errors. These tasks constitute one of the key directions in the development of CAD systems for nanodevices [8, 10-12].

Fig. 1(a) shows a model of a single-electron QCA nanomultiplexer (2 → 1). It is based on three majority elements (MEs) and contains 12 QCA cells of size (18 × 18) nm^2 with a center-to-center spacing of 20 nm. The diameter of the quantum islands is 5 nm, and the overall circuit size is (98 × 98) nm^2 ≈ 0.01 μm^2.

The results of the parametric simulation of the output-cell switching waveforms are illustrated in Fig. 1(b). The varied parameter is the operating temperature, which did not exceed 25 K, not to mention the normal temperature of 273 K. With a slight increase in cryogenic temperature from 0 to 25 K, QCA cells lose the mechanisms of Coulomb blockade and tunneling due to the intensified thermal generation of background electrodes. The amplitudes of pulses numbered 2, 6, 10, and 14 begin to decay especially rapidly. When the nanocircuit is simulated at 28 K, it loses operability altogether, as shown in Fig. 1(c).

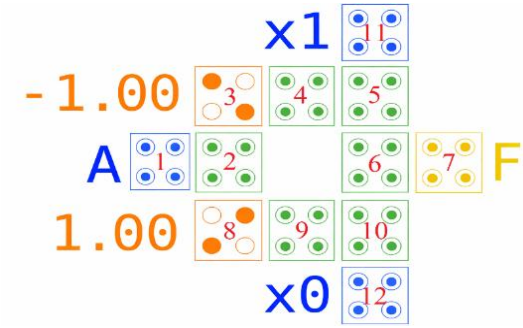

a

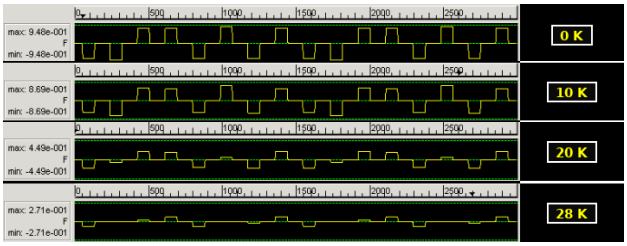

b

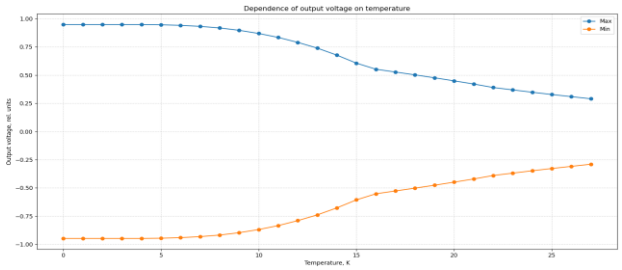

c

Fig. 1 – Simulation of a QCA nanomultiplexer in the QCADesigner workspace: (a) layout; (b) simulation waveforms; (c) degradation (regression) of output characteristics at T = 0-28 K

Table 1 – Truth table nanomultiplexer (2 → 1)

A	x_1	x_0	F
0	0	0	0
0	0	1	0
0	1	0	1
0	1	1	1
1	0	0	0
1	0	1	1
1	1	0	0
1	1	1	1

Fig. 1(d) presents the truth table of the nanomultiplexer, which fully agrees with the obtained waveforms (Fig. 1(b)). From this table, the decimal and canonical forms of the Boolean function were derived:

$$F_{\text{R}} = \sum(010, 011, 101, 111) = \bar{A}x_1\bar{x}_0 \vee \bar{A}x_1x_0 \vee A\bar{x}_1x_0 \vee Ax_1x_0, \quad (3.1)$$

where A – is the single-address input parameter, while x_1, x_0 – are the function arguments applied to the information inputs.

From Boolean Eq. (1), the majority function of the nanomultiplexer comprising three MEs is obtained:

$$F_{\text{M}} = maj[maj(\bar{A}, x_1, 0) \vee maj(A, x_0, 0), 1], \quad (3.2)$$

where maj – is the majority-voting operator that selects the majority value from an odd number of input signals, in this case 2 out of 3.

It follows from Eqs. (3.1) and (3.2) that the multiplexer connects output F to input x_1, when $\bar{A} = 0$, or to input x_0 when $A = 1$, which is consistent with both the waveforms and the truth table. Thus, adequate simulation results were obtained for the nanomultiplexer under cryogenic-temperature conditions.

QCADesigner-E – is an extension of QCADesigner 2.0.3 that makes it possible to perform energy evaluation of QCA nanocircuits on the basis of the Coherence Vector Simulation Engine (CVSE). Simulation in the QCADesigner-E environment generates an Energy Dissipation Report, which reproduces the total energy losses. First, losses occur because of interaction with the surrounding environment [10]:

$$E_{bath\,total} = \sum_{i=1}^{N_{cells}} \frac{1}{2\tau} \int_{t_0}^{t_0+T_{clk}} \left[2\gamma_i \lambda_{x,i} - \Phi_i \lambda_{z,i} - \sqrt{4\gamma_i^2 + \Phi_i^2} \tanh\left(\frac{\sqrt{4\gamma_i^2 + \Phi_i^2}}{2k_B T} \right) \right] dt, \quad (3.3)$$

where N_{cells} – is the number of QCA cells; τ – is the relaxation time; and for the i-th cell: γ_i – is the tunneling energy, $\lambda_{x,i}$, $\lambda_{z,i}$ – are the components of the coherence vector, Φ_i – is the Coulomb-interaction potential with neighboring cells, k_BT – is the thermodynamic potential.

Second, energy losses occur in the clocking conductors [7, 10]:

$$E_{clk\,total} = \sum_{i=1}^{N_{cells}} \left[-\frac{1}{2} \int_{t_0}^{t_0+T_{clk}} \left(\frac{d\gamma}{dt} \lambda_x \right) dt \right], \quad (3.4)$$

where the negative sign of the parameter $E_{clk\,total}$ indicates a possible return of part of the energy during the time interval T_{clk} due to the mutual consistency between the rate of change of the tunneling barrier $\frac{d\gamma}{dt}$ and the coherence vector λ.

Finally, the quantity $E_{Error\,total}$ – is the uncertainty of the energy balance caused by rounding and the finite discretization step during numerical analysis. In general, the energy balance should hold over one T_{clk}, and the deviation from that balance is precisely the uncertainty (error) [7, 10]:

$$E_{Error\,total} = \sum_{i=1}^{N_{cells}} \left(E_{clk}^i + E_{IO}^i - \Delta E^i \right), \quad (3.5)$$

where E_{clk}^i, E_{IO}^i, and $-\Delta E^i$ – are the energy losses in the i-th clock-synchronization interval, during input-output switching, and the correction for changes in stored energy when the clock periodicity ($t_0 + T_{clk}$) has not yet been fully established. After the nanocircuit reaches a steady operating condition, Eq. (5) yields $-\Delta E^i \approx 0$.

In Fig. 2(a), the graph shows that when the 2 → 1 multiplexer is simulated over the temperature range 0-20 K, the energy $E_{bath\,total}$ exhibits a pronounced periodic character. Its values vary approximately within $(4 \div 9) \cdot 10^{-4} eV$. As the temperature rises, a tendency toward increased energy loss and smoother oscillations is observed, which is associated with stronger thermal fluctuations.

The graph in Fig. 2(b) shows that the clocking energy in the nanocircuit also has a distinct periodic character determined by the operation phases of the QCA clocking mechanism. Its values vary approximately within $(3 \div 15) \cdot 10^{-4} eV$. For all temperatures, the periodicity has the same shape: minima correspond to the release/relax phases (partial energy return), whereas maxima correspond to the switch/hold phases (active operation). At the same time, the shape of the dependence remains stable, which confirms correct circuit operation even under temperature influence.

The graphs in Fig. 2(c) illustrate that within the temperature range 0-20 K the absolute simulation error does not exceed $10^{-4} eV$ and shows no signs of accumulation. This indicates the stability and correctness of the computational process and provides grounds to consider the obtained energy dependences reliable. All values are negative and lie within the narrow range $-(10 \div 5{,}5) \cdot 10^{-5} eV$. The sign here has no physical meaning; it merely indicates the direction of the numerical energy-balance residual. If an even smaller error is required, it is usually reduced by adjusting the integration step used in the calculations.

The three graphs in Fig. 2(d) demonstrate periodic variations of the energies $E_{bath\,total} = (5{,}11 \div 8{,}77) \cdot 10^{-4} eV$, $E_{clk\,total} = (1{,}5 \div 3{,}1) \cdot 10^{-4} eV$ and $E_{Error\,total} = -(5{,}3 \div 9{,}32) \cdot 10^{-4} eV$ for QCA cells, which are associated with the cyclic nature of the synchronization of the multiplexer nanocircuit.

In Fig. 3(a), the $Sum_{E_{bath}}$ graph shows that the total energy losses of the nanomultiplexer to the surrounding environment in the range $(0 \div 15) K$ increase up to $0{,}011\ eV$ near 15 K. This is explained by thermal exchange with the environment. At 20 K, a decrease in E_{bath} to $9{,}9 \cdot 10^{-3} eV$ is observed. In general, the results confirm that increasing temperature mostly leads to a growth of energy dissipated into the environment; however, for a correct confirmation of the non-monotonic behavior at 20 K, it would be desirable to increase the number of points/runs or refine the dissipation estimate.

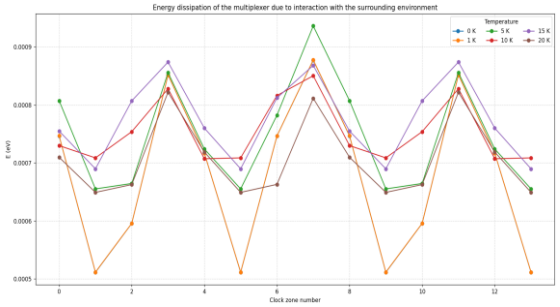

a

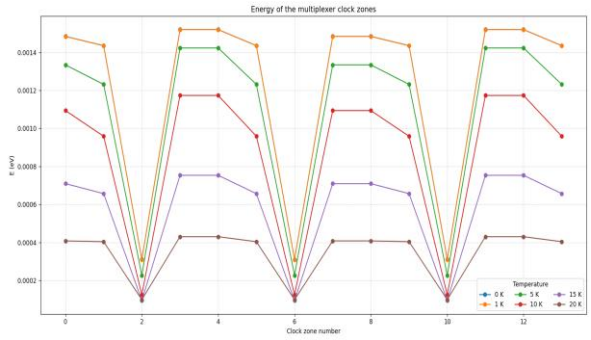

b

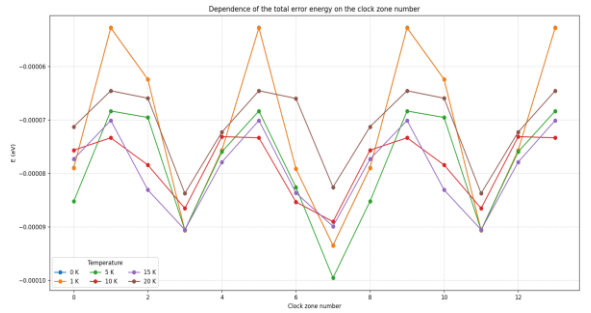

c

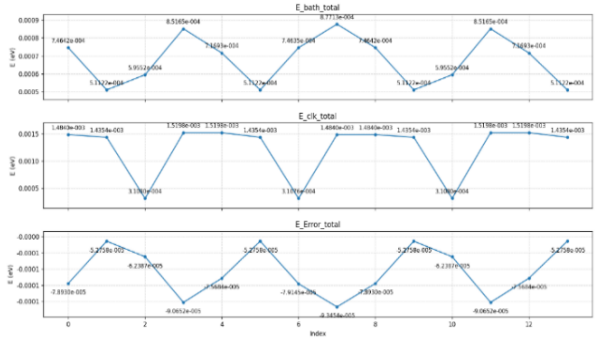

d

Fig. 2 – Energy losses of the nanomultiplexer at $T = 0$, 1, 5, 10, 15, and 20 K: dissipation due to interaction with the surrounding environment (a), clocking zones (b), and simulation errors (c); energy distribution across cells at $T = 0$ K (d)

The average dissipation energy E_{bath} changes in a similar way, as shown in Fig. 3(b), while the nanocircuit retains stable operation.

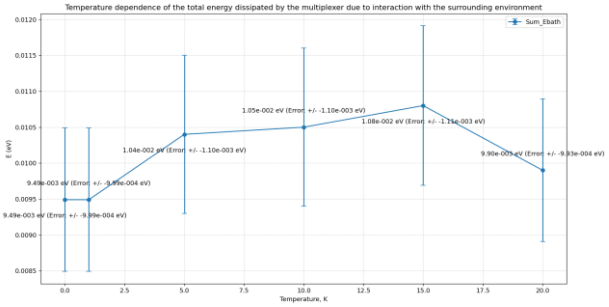

a

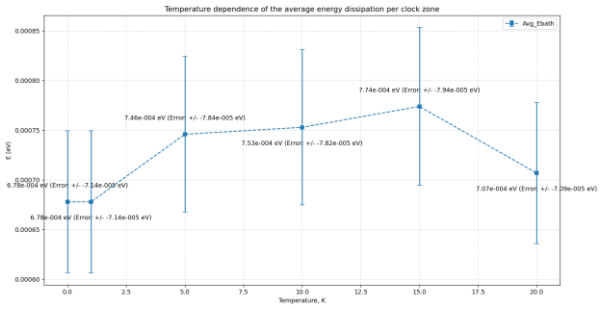

b

Fig. 3 – Temperature dependences of the total Sum_{Ebath} (a) and average E_{bath} (b) dissipation energy of the (2 → 1) multiplexer nanocircuit

QCADesigner-FS – is a specialized version of the previously mentioned single-electronics CAD tools supplemented with a fault-simulation block, for example, for evaluating the influence of dislocations or lattice vacancies. For this purpose, repeated simulation of the nanocircuit is performed at a specified probability – for example, 1, 10, 30, and 50 % – for each of four types of defects that cause errors in the interaction of conduction electrons with defects in low-dimensional structures: vacancy, interstitial, dopant, and dislocation. Such an approach is necessary because QCA parameters are quite sensitive to these process-induced deviations, which primarily affect the polarization interaction between cells [4, 17]. Defect simulation is carried out both deterministically and randomly in order to identify especially critical nanocircuit regions and to enable their redesign [11]. Process engineers and designers must have experience in optimal cell placement and, in particular, in tuning the phase alignment of clocking zones, which suppresses faults and improves reliability, especially in large QCA nanocircuits [9, 12].

The probability of correct execution of functions (1) and (2) by the single-electron multiplexer shown in Fig. 1(a) is determined from the simulation results for the distribution of errors in Fig. 4, caused by the influence of nanoscale structural defects on electrons. These defects include vacancies, i.e., the complete absence of a cell (a); interstitial defects, or displacement of a defective cell by 1–100% (b); dopants, i.e., random removal of a quantum dot from a cell (c); and dislocations, or cell rotation by $1 \div 360°$ (d).

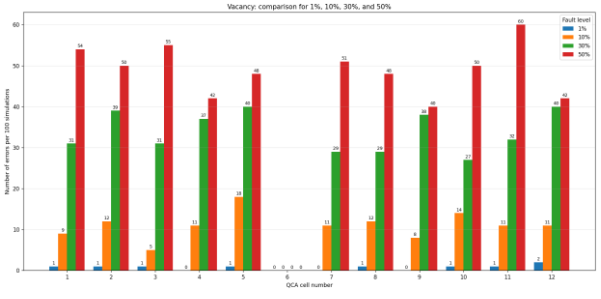

a

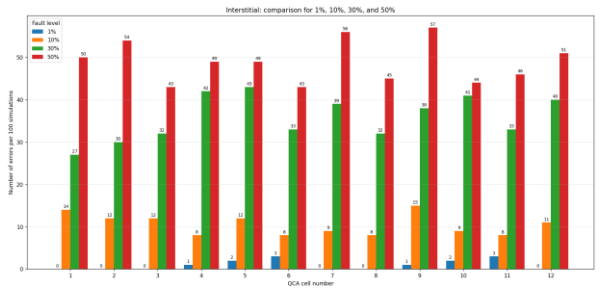

b

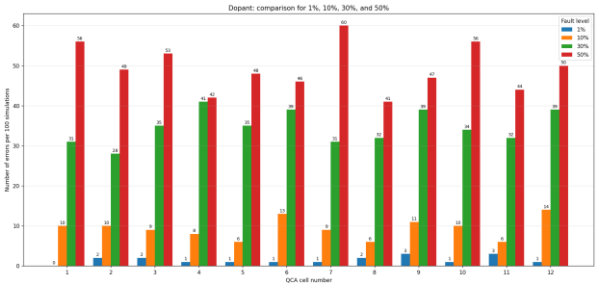

c

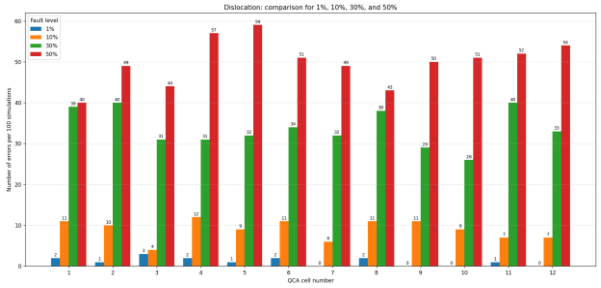

d

Fig. 4 – Distribution of the number of errors over all cells of the nanomultiplexer under the action of vacancy (a), interstitial (b), dopant (c), and dislocation (d) mechanisms at fault probabilities of 1%, 10%, 30%, and 50%, respectively

Mathematical processing of stochastic error information is implemented using the Monte Carlo procedure. The CAD system iteratively introduces defects and launches the base simulation, comparing the obtained parameters of the defective nanocircuit with the reference one.

The graphs in Fig. 4 show that at a defect probability of 1%, the errors are isolated in individual cells and do not lead to failures. At 10 %, a stable pattern of locally vulnerable cells is already formed: input cell 2, upper working cell 5, and output cell 7. At a defect level of 30%, errors spread over the entire nanostructure, and at 50% the circuit rapidly loses operability.

The most destructive vacancy-induced defects affect cells 2, 4, 5, and 12. At 50 %, the maximum error value is reached in cell 11 (60 errors over 100 simulation cycles). For interstitial defects, a more uniform growth of errors is characteristic and is observed practically over the entire topology in regions 4-5, 7, 9-10, 11, and 12. The graphs for dopants demonstrate an intensive increase in errors in almost all cells and a rapid spread of instability, which is why these defects are usually considered the most destructive. The dislocation distribution indicates that the disturbance of the geometric positions of cells is most dangerous for the internal switching paths (cells 2, 5, 6, and 10).

Thus, the most vulnerable cells are those that receive the address input signal $A(cells\ 1\ and\ cells\ 2)$, control the majority decisions for the information signals $x_1(cells\ 11)$ and $x_0(cells\ 12)$ and form the output $F(cells\ 7)$.

At this stage of automated design, the experience of circuit designers and process engineers makes it possible to create highly reliable large-scale nanocircuits.

4. PROSPECTS FOR FURTHER RESEARCH

The authors believe that further studies should be directed toward expanding the range of modern single-electron nanocircuits based on QCA, in particular toward the analysis of more complex combinational and sequential nodes, in which the influence of temperature, energy dissipation, and structural defects may manifest itself differently than in the (2 → 1) nanomultiplexer. Another important direction is to refine the operability limits of such circuits over a wider range of simulation parameters, including temperature conditions, clocking-zone configurations, geometric characteristics of cells, and features of their spatial arrangement. This will make it possible to evaluate more deeply the relationship between nanocircuit topology, functional stability, and energy efficiency.

5. CONCLUSIONS

The study confirms that the computer-aided design of single-electron QCA nanocircuits is an effective approach for investigating their functional, energy, and reliability characteristics. The constructed (2 → 1) nanomultiplexer correctly implements the specified logical function; however, its operation depends strongly on temperature: as temperature increases, the output characteristics degrade, and near 25-28 K the circuit loses operability. Energy simulation showed an increase in losses to the environment with increasing temperature while maintaining a small numerical calculation error.

The defect-tolerance analysis showed that the investigated circuit is nonuniform in its vulnerability to structural defects. The largest numbers of errors are caused by defects in the cells responsible for receiving the input signal, polarization, control, and output formation. It was established that random quantum-dot removal defects (Dopant) and cell rotation defects (Dislocation) are the most destructive for the internal signal-transfer paths; defective-cell displacement (Interstitial) affects the topology more uniformly; and cell absence (Vacancy) most clearly reveals both critical and anomalously stable cells. This confirms the need for topological optimization specifically of the functionally important nodes of the circuit.

REFERENCES

1. H. Grabert, M.H. Devoret, et al, *NATO ASI Series B: Physics* **294**, (1992) https://doi.org/10.1007/978-1-4757-2166-9.
2. K.K. Likharev, *Proc. IEEE* **87** No 4, 606 (1999) http://doi.org/10.1109/5.752518.
3. P. Papadopoulou, K. Ovaliadis, E. Philippousi, M.P. Hanias, L. Magafas, S.G. Stavrinides, *Symmetry* **16** No 3, (2024) https://doi.org/10.3390/sym16030327.
4. U. Mehta, V. Dhare, *Quantum-Dot Cellular Automata (QCA): A Survey* [Електронний ресурс]. (2017) https://arxiv.org/pdf/1711.08153.
5. P.D. Tougaw, C.S. Lent, *J. Appl. Phys.* **75** No 3, 1818 (1994) https://doi.org/10.1063/1.356375.
6. K. Hennessy, C.S. Lent, *J. Vac. Sci. Technol. B* **19** No 5, 1752 (2001) https://doi.org/10.1116/1.1387088.
7. J. Timler, C.S. Lent, *J. Appl. Phys.* **91** No 2, 823 (2002) https://doi.org/10.1063/1.1421217.
8. K. Walus, T.J. Dysart, G.A. Jullien, R.A. Budiman, *IEEE Trans. Nanotechnology* **3** No 1, 26 (2004) https://doi.org/10.1109/TNANO.2003.820815.
9. C.S. Lent, M. Liu, Y. Lu, *Nanotechnology* **17** No 16, 4240 (2006) https://doi.org/10.1088/0957-4484/17/16/040.
10. F.S. Torres, R. Wille, P. Niemann, R. Drechsler, *IEEE Trans. Comput.-Aid. Design Integrated Circ. Syst.* **37** No 12, 3031 (2018) https://doi.org/10.1109/TCAD.2018.2789782.
11. D.A. Reis, F.S. Torres, *Proceedings of the 28th Symposium on Integrated Circuits and Systems Design (SBCCI)*, 15:1 (2015) https://doi.org/10.1145/2800986.2800995.
12. D. Bhowmik, J. Pal, M. Goswami, P. Sen, A.K. Saha, B. Sen, *IET Circ., Dev. Syst.* **15** No 2, 156 (2021) https://doi.org/10.1049/cds2.12015.
13. C.A.T. Campos, A.L. Marciano, O.P.V. Neto, F.S. Torres, *IEEE Trans. Comput.-Aid. Design Integrated Circ. Syst.* **35** No 3, 513 (2016) https://doi.org/10.1109/TCAD.2015.2471996.
14. M. Goswami, A. Mondal, M.H. Mahalat, B. Sen, B.K. Sikdar, *Int. J. Electron. Lett.* **8** No 1, 83 (2020) https://doi.org/10.1080/21681724.2019.1570551.
15. V. Vankamamidi, M. Ottavi, F. Lombardi, *IEEE Trans. Comp.-Aid. Design Integrated Circ. Syst.* **27** No 1, 34 (2008) https://doi.org/10.1109/TCAD.2007.907020.
16. Navidi, R. Sabbaghi-Nadooshan, M. Dousti, *Scientia Iranica. Trans. D* **29** No 6, 3249 (2022) https://doi.org/10.24200/sci.2021.53471.3256.
17. *Field-Coupled Nanocomputing: Paradigms, Progress, and Perspectives* – VIII, 393 p. – (LNCS, vol. 8280) (Eds. by N.G. Anderson, S. Bhanja) (Berlin; Heidelberg: Springer: 2014) https://doi.org/10.1007/978-3-662-43722-3.
18. R. Landauer, *IBM J. Res. Develop.* **5** No 3, 183 (1961) https://doi.org/10.1147/rd.53.0183.
19. C.H. Bennett, *IBM J. Res. Develop.* **17** No 6, 525 (1973) https://doi.org/10.1147/rd.176.0525.
20. T. Heinzel, Mesoscop. Electron. Solid State Nanostruct. **9**, 247 (2007).
21. J. Timler, C.S. Lent, *J. Appl. Phys.* **94** No 2, 1050 (2003) https://doi.org/10.1063/1.1581350.

Сучасні інструменти САПР для одноелектронних нанопристроїв

О.С. Мельник, О.О. Нагайченко

Національний університет «Київський авіаційний інститут», 03058 Київ, Україна

Представлено аналіз результатів, отриманих у процесі автоматизованого проектування нанопристроїв на основі квантово-точкових клітинних автоматів з використанням сучасних одноелектронних САПР, таких як QCADesigner, QCADesigner-E та QCADesigner-FS. На прикладі схеми наномультиплексора було проведено функціональне, температурно-залежне, термоенергетичне та ймовірнісне дефектоорієнтоване моделювання. Показано, що сучасні пакети САПР дозволяють не тільки синтезувати топологію наносхеми, але й всебічно оцінити її працездатність, енергоефективність та стійкість до структурних дефектів. Зрештою було встановлено, що досліджуваний наномультиплексор коректно реалізує функцію селекції сигналу; однак він залишається працездатним лише в обмеженому кріогенному діапазоні температур. Енергетичний аналіз виявив періодичну поведінку компонентів дисипації, пов'язаних з фазами тактування, тоді як моделювання за допомогою QCADesigner-FS підтвердило значну залежність ймовірності помилки від чотирьох типів дефектів, викликаних процесом, рівня несправності та топологічного розміщення комірок. Найбільш вразливими елементами виявилися функціонально критичні вузли, пов'язані з введенням сигналу, керуванням та формуванням виходу.

Ключові слова: Одноелектронна наноелектроніка, Автоматизоване проєктування, Кріогенна температура, Дисипація енергії, Дефектостійкість наносхем.